



## OPEN

SUBJECT AREAS:  
NANOCAVITIES  
METAMATERIALSReceived  
2 September 2014Accepted  
30 December 2014Published  
2 February 2015Correspondence and  
requests for materials  
should be addressed to  
K.A. (aydin@  
northwestern.edu) or  
H.K. (drhasankocer@  
gmail.com; hkocer@  
kho.edu.tr)

# Reduced near-infrared absorption using ultra-thin lossy metals in Fabry-Perot cavities

Hasan Kocer<sup>1,2</sup>, Serkan Butun<sup>1</sup>, Zhongyang Li<sup>1</sup> & Koray Aydin<sup>1</sup><sup>1</sup>Department of Electrical Engineering and Computer Science, Northwestern University, Evanston, IL 60208, USA, <sup>2</sup>Department of Electrical Engineering, Turkish Military Academy, 06654 Ankara, Turkey.

We show that a triple-layer metal-insulator-metal (MIM) structure has spectrally selective IR absorption, while an ultra-thin metal film has non-selective absorption in the near infrared wavelengths. Both sub-wavelength scale structures were implemented with an ultra-thin 6 nm Cr top layer. MIM structure was demonstrated to have near perfect absorption at  $\lambda = 1.2 \mu\text{m}$  and suppressed absorption at  $\lambda = 1.8 \mu\text{m}$  in which experimental and simulated absorptions of the thin Cr film are even higher than the MIM. Occurrence of absorption peaks and dips in the MIM were explained with the electric field intensity localization as functions of both the wavelength and the position. It has been shown that the power absorption in the lossy material is a strong function of the electric field intensity i.e. the more the electric field intensity, the more the absorption and vice versa. Therefore, it is possible to engineer IR emissive properties of these ultra-thin nanocavities by controlling the electric field localization with proper designs.

Fabry-Perot (FP) optical cavities and coatings are widely used in optoelectronic devices such as solar cells, photo-detectors, lasers, interference filters, and spectrometers<sup>1</sup>. In a conventional FP cavity, two mirrors are separated by at least a quarter-wavelength thick lossless dielectric spacer. Depending on the thickness of the dielectric spacer the incident light interferes constructively or destructively with the reflected light, therefore one can control the intensity of reflected and transmitted electromagnetic waves. Here, we demonstrate that by utilizing an ultra-thin lossy metal film as the top layer of a Fabry-Perot film, one can increase and decrease the absorption amplitude of an ultrathin Cr film significantly. Controlling and manipulating the spectral absorption properties of materials is an active area of research. In particular, metamaterial and plasmonic nanostructure based absorbers were studied extensively for achieving perfect or near-perfect absorption of electromagnetic radiation at microwave<sup>2</sup>, terahertz<sup>3</sup>, infrared<sup>4–6</sup> and visible<sup>7</sup> wavelengths. These micro or nanostructured absorbers are very thin compared to the operating wavelength, however they often require complex, time-consuming and expensive nanofabrication steps. Recently, use of continuous, lithography-free lossy metallic or semiconducting films<sup>8–10</sup> has opened new ways for using ultra-thin sub-wavelength interference films with the advantage of simple fabrication steps. Ultra-thin lossy films with thickness-dependent absorption properties have been demonstrated at visible<sup>9,11</sup> visible and near-infrared<sup>12–14</sup> and mid-infrared<sup>8,15–17</sup> spectral regions.

In this study, we demonstrated enhanced or reduced absorption with an ultra-thin (6 nm thick) lossy Cr metal film. The absorption of a thin Cr film at near-IR wavelengths is compared to the absorption of an MIM Fabry-Perot cavity with a 590 nm thick PMMA dielectric spacer layer. We observe almost-perfect IR absorption at  $\lambda = 1.2 \mu\text{m}$  as well as reduced absorption at  $\lambda = 1.8 \mu\text{m}$ . Although enhanced absorption can be easily achieved using nanostructured resonators, reducing the absorption of a specific material is a challenging task. Reducing absorption will result in reduced thermal emission therefore IR radiation from a surface can be suppressed significantly using lossy MIM Fabry-Perot cavity that we propose in this paper.

## Results

**Proposed designs.** We investigated the absorption properties of an ultra-thin Cr metal film on a sapphire substrate (Fig. 1(a)) and in a Fabry-Perot type metal-insulator-metal (MIM) optical cavity (Fig. 1(b)). A lossy 6 nm-thick chromium (Cr) metal is the top layer of both structures. Additionally, MIM has a lossless dielectric spacer made up of Poly(methyl methacrylate) (PMMA) in the middle and a lossy thick gold (Au) at the bottom layers, respectively. Sapphire substrate was chosen because of its excellent transmittance up to 6  $\mu\text{m}$ . Chromium is a lossy metal and absorbs ~20–30% of near-infrared radiation depending on its thickness. When a thin Cr layer is used as the top

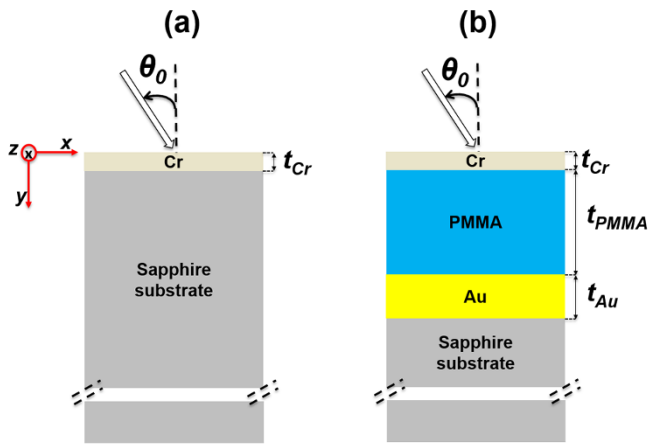


**Figure 1** | (a) Thin Cr film.  $t_{Cr} = 6$  nm. (b) MIM structure.  $t_{Cr} = 6$  nm,  $t_{PMMA} = 590$  nm and  $t_{Au} = 100$  nm.

layer of an MIM cavity as shown schematically in Fig. 1(b), the incident light will pass through the Cr layer and will travel along the distance of the spacer layer and reflect back from the optically thick gold mirror. The electric field intensities in the Cr and Au metals can be controlled by the thickness of the dielectric spacer layer. In this study, the thickness of the dielectric layer is fixed at 590 nm.

Analytical simulations were based on the Transfer Matrix Method (TMM)<sup>18</sup>. Incidence angle and polarization parameters were included in the TMM model. In this method, following matrix formulation were developed in accordance with our structures

$$\begin{pmatrix} M_{11} & M_{12} \\ M_{21} & M_{22} \end{pmatrix} = D_{12}P_2D_{23}P_3D_{34}P_4D_{45} \quad \text{for MIM} \quad (1)$$

$$= D_{12}P_2D_{23} \quad \text{for thin Cr film}$$

Here, the transmission matrices ( $D_{i,i+1}$ ,  $i = 1..4$  for MIM and  $1..2$  for thin Cr film) are modeled by

$$D_{i,i+1} = \frac{1}{t_{i,i+1}} \begin{bmatrix} 1 & r_{i,i+1} \\ r_{i,i+1} & 1 \end{bmatrix} \quad (2)$$

where  $r_{i,i+1}$  and  $t_{i,i+1}$  are Fresnel reflection and transmission coefficients. The incidence angle and the polarization are modeled using these coefficients as follows

for TE or s wave angular incidence

$$r_{i,i+1} = \frac{\tilde{n}_i \cos \theta_i - \tilde{n}_{i+1} \cos \theta_{i+1}}{\tilde{n}_i \cos \theta_i + \tilde{n}_{i+1} \cos \theta_{i+1}} \quad (3)$$

$$t_{i,i+1} = \frac{2\tilde{n}_i \cos \theta_i}{\tilde{n}_i \cos \theta_i + \tilde{n}_{i+1} \cos \theta_{i+1}} \quad (4)$$

for TM or p wave angular incidence

$$r_{i,i+1} = \frac{\tilde{n}_i \cos \theta_{i+1} - \tilde{n}_{i+1} \cos \theta_i}{\tilde{n}_i \cos \theta_{i+1} + \tilde{n}_{i+1} \cos \theta_i} \quad (5)$$

$$t_{i,i+1} = \frac{2\tilde{n}_i \cos \theta_i}{\tilde{n}_i \cos \theta_{i+1} + \tilde{n}_{i+1} \cos \theta_i} \quad (6)$$

Propagation matrices ( $P_i$ ,  $i = 2..4$  for MIM and  $2$  for thin Cr film) are modeled by

$$P_i = \begin{bmatrix} e^{-j\phi_i} & 0 \\ 0 & e^{j\phi_i} \end{bmatrix} \quad (7)$$

$\phi_i = \frac{2\pi}{\lambda} \tilde{n}_i h_i \cos \theta_i$  is the phase shift,  $\tilde{n}_i = n_i + jk_i$  is the complex refractive index,  $h_i$  is the thickness of the  $i$ th layer, and  $\theta_i$  is the refraction angle in the  $i$ th layer.

Reflection and transmission are computed using  $R = \left| \frac{M_{21}}{M_{11}} \right|^2$  and  $T = \frac{n_s \cos \theta_s}{n_0 \cos \theta_0} \left| \frac{1}{M_{11}} \right|^2$ . Here,  $n_o$  and  $n_s$  are the refractive indices of top air and bottom sapphire substrate.  $\theta_0$  is the incidence angle on the top of the structures while  $\theta_s$  is the refracted angle inside the substrate.

**Effect of Cr thickness.** Both Finite-Difference Time-Domain (FDTD) and TMM techniques were used for electromagnetic simulations. A plane wave source is assumed to be normally incident and propagate along  $x$ -axis through the structures. We made simulations to understand the effect of the top Cr layer thickness on the absorption spectra. Complex refractive indices for Cr and Au were taken from the Palik database<sup>19</sup>. Index of the PMMA and sapphire were set to constant values of 1.47 and 1.7, respectively since these layers were assumed to be lossless in our spectral range of interest. The thickness of the top Cr layer was changed from 0 to 20 nm with 1 nm step size. Transmitted and reflected power from the absorbers are computed using transmission and reflection power monitors and absorption is calculated by using the equation

$$A(\lambda) + R(\lambda) + T(\lambda) = 1 \quad (8)$$

where  $A(\lambda)$ ,  $R(\lambda)$  and  $T(\lambda)$  are absorption, reflectivity and transmittance, respectively.

Simulation results are plotted in Fig. 2. The thin Cr film has a fairly constant, non-resonant absorption (Fig. 2(a)), whereas the absorption spectra of MIM film demonstrates resonant absorption behavior, as can be seen from the absorption peaks and dips (Fig. 2(b)). For a 0 nm thick top Cr film, the MIM film essentially becomes a gold mirror coated with a spacer layer, therefore most of the incident light is reflected back with little absorption, and resonant behavior is not observed. Increasing the Cr thickness results in pronounced absorption peaks and dips throughout the wavelength of interest, due to the Fabry-Perot resonant cavity. For a 20 nm thick Cr film, transmission through the Cr layer is significantly reduced, therefore Fabry-Perot resonance becomes weaker and the absorption intensity reduces. Our simulations provided an optimal point for 6 nm top Cr layer, at 1.2  $\mu\text{m}$ , where we observed almost-perfect absorption with an absorption value of 0.99. On the other hand, around  $\lambda = 1.8 \mu\text{m}$ , the absorption in the MIM structure is suppressed for all Cr thicknesses to a value that is well below the absorption in the thin Cr film.

Consequently, the MIM and thin Cr film absorbers were fabricated with 6 nm thick top Cr layer. Two different absorbers, which are schematically shown in Fig. 1, were experimentally realized by electron beam deposition on double side polished sapphire substrates. We will refer these two different metallic films “thin Cr film” and “MIM” for the rest of this paper. MIM (Fig. 1(b)) is a triple-layer metal-insulator-metal (MIM) while thin Cr film (Fig. 1(a)) is just a one layer of absorber on a transparent substrate.

**Comparisons of measurements and simulations.** In Fig. 3, we plot the measured, and simulated absorption spectra of MIM and thin Cr films. In this study, experimental transmission of thin Cr films was measured using Fourier transform infrared (FTIR) spectrometer (Bruker Vertex 70) equipped with a room temperature triglycine sulfate (DTGS) detector. We did not measure transmission of MIM because it has an optically thick 100 nm Au bottom metal, which prevents the light transmission. Experimental reflection measurements of both structures were carried out using an infrared microscope (Bruker Hyperion 2000) and the same FTIR spectrometer with liquid nitrogen cooled mercury cadmium telluride (HgCdTe) detector.

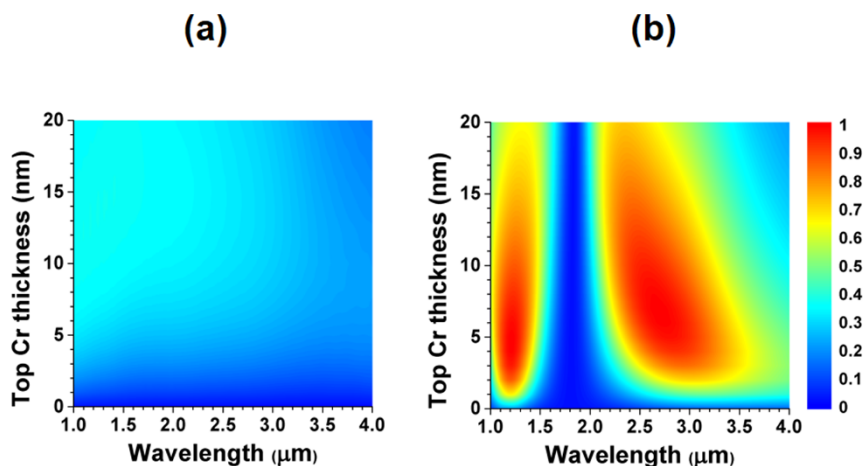


**Figure 2** | Absorption map with respect to top Cr thickness sweep for (a) thin Cr film and (b) MIM structure with same scale colorbar as seen on the right.

As illustrated in Fig. 3, we obtained a remarkably good agreement between simulations and experiments in terms of predicting the resonant peak and dip positions between 1.1 and 2.1  $\mu\text{m}$  wavelength range in the absorption spectrum. Beyond 2.1  $\mu\text{m}$  wavelength, there is a slight deviation in experimental absorption spectrum of the MIM from simulations. This might have been resulted from two facts. Firstly, ultra-thin (6 nm) Cr index of the experimental MIM structure might be somehow different than the bulk index of the Ref. 19. Secondly, experimental PMMA index beyond 2.1  $\mu\text{m}$  wavelength

may exhibit dispersive and lossy characteristics instead of the constant one, which was not considered in our simulations.

Within this spectral range, we observed that the MIM has two contradictory behaviors such that it has increased absorption approaching the near perfect condition at  $\lambda = 1.2$  and suppressed absorption at  $\lambda = 1.8$   $\mu\text{m}$  compared to the relatively constant absorption spectrum of the thin Cr film. Increased absorption of the MIM relative to the thin Cr film is somewhat trivial. It can be attributed to the electric field confinement and enhancement within the Fabry-Perot type MIM nanocavity structure. On the other hand, second case, which is the suppression of the absorption within the same structure relative to the bare thin Cr film is rather nontrivial.

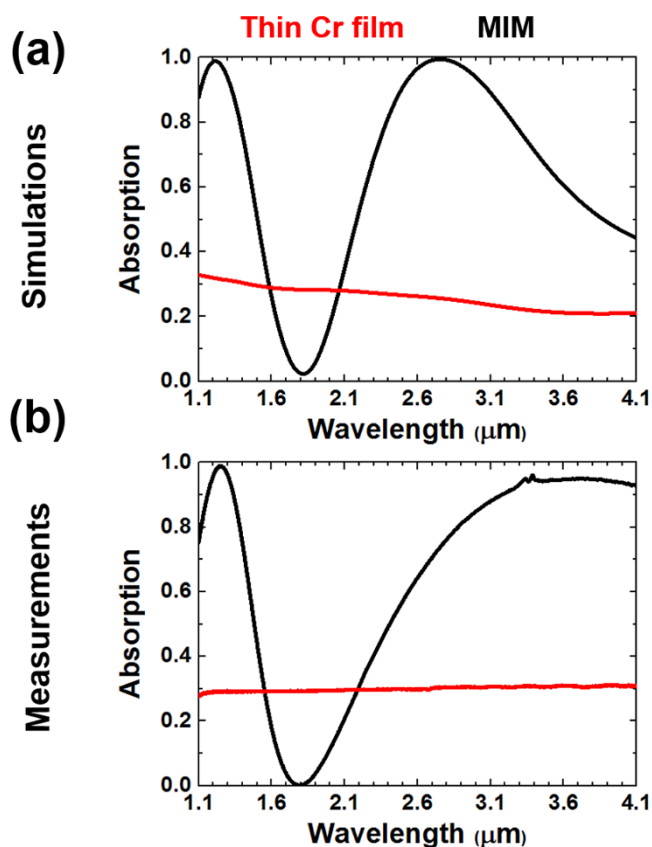


**Figure 3** | Absorption spectra of the thin Cr film (represented by red color) and the MIM structures (represented by black color). Both structures shown in Fig. 1 have 6 nm top Cr thicknesses. (a) Simulations with TMM method. (b) Measurements with FTIR.

**Effect of incident angle and polarization.** The angular dependence of absorption spectra for TE and TM polarizations were calculated using TMM within the thin Cr film and the MIM structures of Fig. 1. In TE polarization, the electric field is normal to the incidence plane ( $x$ - $y$  plane), whereas it is inside the incidence plane in TM polarization. We note that the near perfect and the reduced absorption behaviors are almost same within an angular incidence of up to  $40^\circ$  for both polarizations while the resonant dip and peak positions of the MIM were slightly blue shifted (Fig. 4 (a)–(c)). If the incident angle is further increased to  $60^\circ$ , the absorption peaks of the MIM reduce and both peaks and dips shift to lower wavelengths for TE and TM polarizations. On the other hand, nonselective spectral absorption intensity of the thin Cr film is relatively higher in TM case as shown in Fig. 4 (d).

**Absorption mechanisms of the structures.** In order to explain reduced absorption mechanism, electric field intensities were calculated using FDTD simulations. Then, the resulting absorbed power density ( $P_{abs}$ ) and electric field intensity ( $|E|^2$ ) inside the structures were plotted in Figs. 5 (a) and (b).  $P_{abs}$  is the divergence of the Poynting vector for non-magnetic materials and can easily be calculated using the simple relation of

$$P_{abs} = \frac{1}{2} \omega \text{Im}(\epsilon) |E|^2 \quad (9)$$

where  $\omega$  is the angular frequency,  $\text{Im}(\epsilon)$  is the imaginary part of the dielectric permittivity and  $|E|$  is the magnitude of the total electric field<sup>7,20</sup>.

When we look at the absorbed power plot (Fig. 5 (a)), we note that dominant absorption occurs inside the 6 nm thick lossy Cr top layer for both MIM and thin Cr film. For the MIM structure, there is slight absorption in the bottom Au layer, however this is significantly smaller than the light absorption occurring in the top Cr layer because field penetration into the optically thick Au layer is minimal.

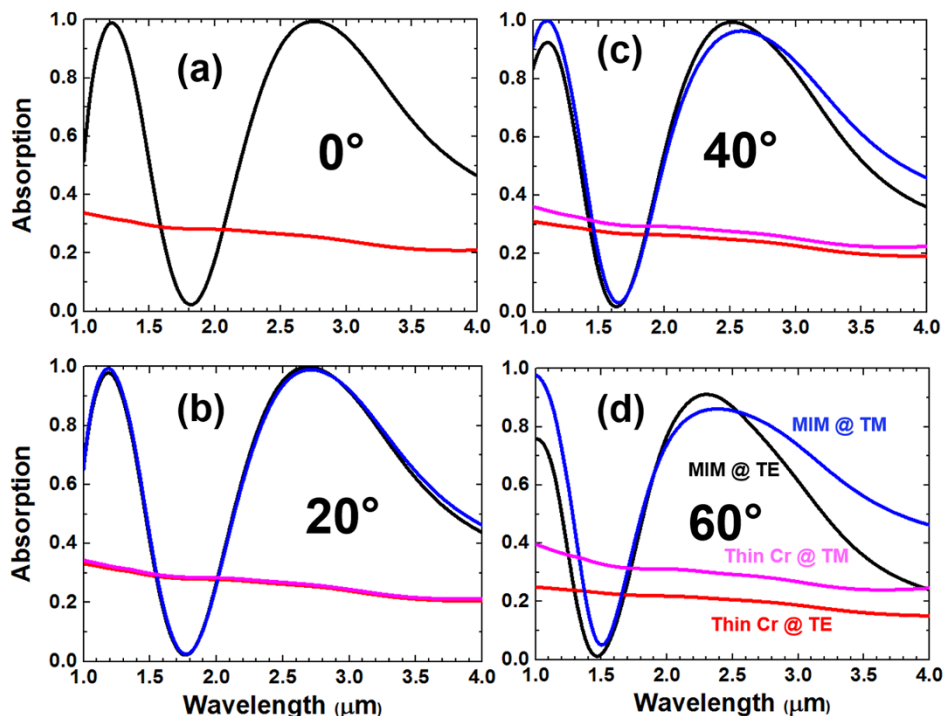


**Figure 4** | Absorption spectra of the thin Cr film and the MIM structures for TE and TM polarizations at different incident angles. TE and TM polarizations of the MIM are represented by black and blue colors, respectively while the polarizations of the thin Cr film are represented by red and magenta colors, respectively. (a) Incidence angle,  $\theta_0 = 0^\circ$  (normal incidence). (b)  $\theta_0 = 20^\circ$ . (c)  $\theta_0 = 40^\circ$ . (d)  $\theta_0 = 60^\circ$ .

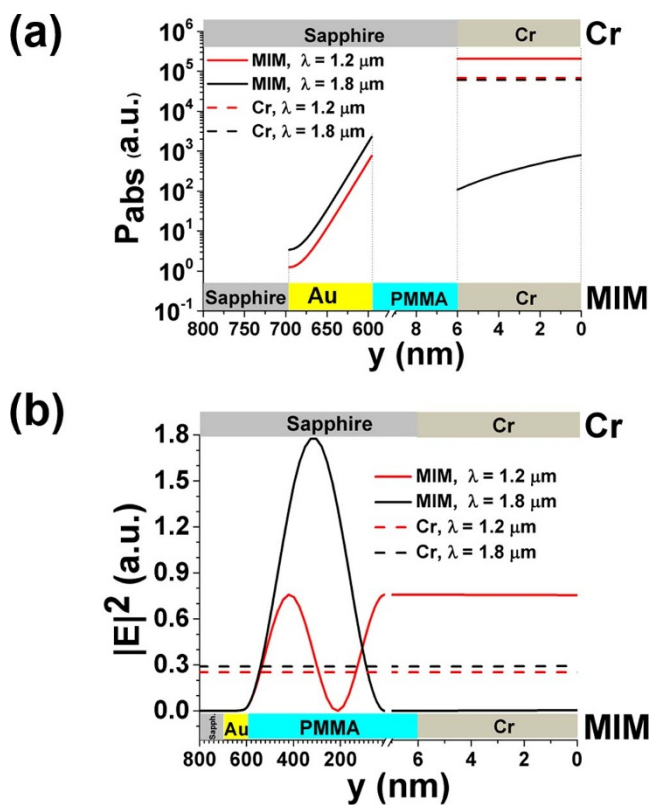


**Figure 5** | Incidence angle,  $\theta_0 = 0^\circ$  (normal incidence) (a) Absorbed power density inside the MIM and thin Cr film at  $\lambda = 1.2$  &  $1.8 \mu\text{m}$  wavelengths. (b) Electric field intensity inside the MIM and thin Cr film at  $\lambda = 1.2$  &  $1.8 \mu\text{m}$  wavelengths.

$P_{abs}$  of the thin Cr film is almost same at both wavelengths of interest whereas  $P_{abs}$  ( $\lambda = 1.2 \mu\text{m}$ ) of the MIM is much higher (approximately 500 times) than  $P_{abs}$  ( $\lambda = 1.8 \mu\text{m}$ ) of the MIM and higher (approximately 3 times) than  $P_{abs}$  ( $\lambda = 1.2$  &  $1.8 \mu\text{m}$ ) of the thin Cr film. The reason for these absorption differences within the same geometry and the same material is better understood by examining the electric field intensity distribution as depicted in Fig. 5(b). Here, we observe two important physical behaviors. One is the confinement of the electric fields inside the sub wavelength scale MIM nanocavity structure as a standing wave between the optically thick bottom Au metal reflector and the ultra-thin lossy top Cr layer. This confinement of the field varies with respect to the wavelength and the thickness of the dielectric spacer. The 6 nm top Cr layer of the MIM is positioned at a peak (highest intensity) point of the second confined mode of the electric field at  $1.2 \mu\text{m}$ , whereas it is positioned at the null point of the first confined mode of the electric field at  $1.8 \mu\text{m}$ . Other physical behavior is related to the thin Cr film. Since this structure has only one lossy layer and does not have any bottom reflector, the electric field is not like the standing-wave style but is like a travelling wave type, so field and intensity distribution inside the top lossy layer of this structure is more likely to be wavelength insensitive. As a result, it has approximately constant, but higher than the MIM field intensity at  $\lambda = 1.8 \mu\text{m}$  wavelength as illustrated in the Fig. 5 (b).

**Spectral thermal emissivity.** Spectral selectivity is an important requirement from target recognition to bio-chemical sensing applications<sup>21</sup>. IR emissive and absorptive properties of a material can be controlled by the reflectivity and transmittance properties of the optical material which depend on the material geometry and optical parameters of the material. In addition to engineering absorptivity, one can also engineer the thermal emissivity using the equation

$$M(\lambda, T) = \varepsilon(\lambda) \frac{2\pi hc^2}{\lambda^5 (e^{\frac{hc}{\lambda kT}} - 1)} \quad (10)$$



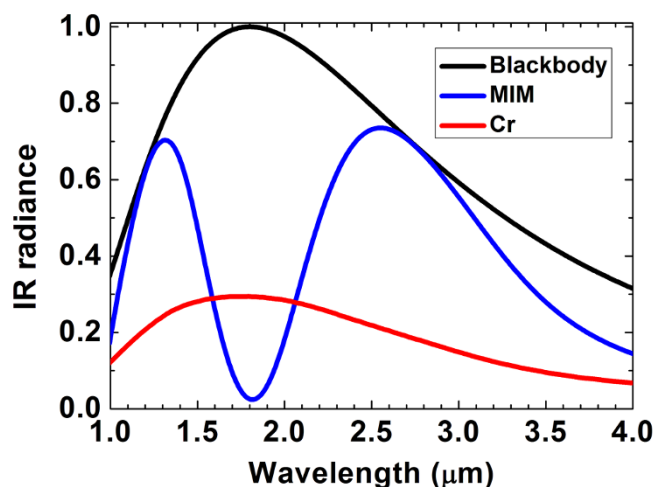


**Figure 6** | IR spectral radiance comparison of the ideal blackbody, MIM and thin Cr film at  $T = 1610$  K, which corresponds to  $\lambda = 1.8 \mu\text{m}$  peak emission wavelength of the ideal blackbody. IR radiances of all three plots are normalized with respect to maximum radiance value of the ideal blackbody at  $\lambda = 1.8 \mu\text{m}$ .

where  $M(\lambda, T)$  is the spectral radiance,  $c$  is the speed of light,  $h$  is the Planck's constant,  $k$  is the Boltzmann's constant,  $T$  is the temperature and  $\varepsilon(\lambda)$  is the wavelength and material/geometry dependent emissivity. Here, the emissivity,  $\varepsilon(\lambda)$ , is the key parameter since it directly affects the wavelength selectivity and spectral intensity. Numerous applications such as camouflage, infrared (IR) signature mimicry, imaging, sensors, IR labeling and wavelength selective IR sources<sup>15,21</sup> can be realized by controlling and engineering the emissivity. Kirchhoff's law of thermal radiation states that the emissivity of a material is equal to its absorption,  $A(\lambda)$ , at thermal equilibrium in which following relation holds<sup>22</sup>

$$\varepsilon(\lambda) = A(\lambda) = 1 - R(\lambda) - T(\lambda) \quad (11)$$

Utilizing equation (10) and (11), the spectral absorption (which equals to the emissivity) of the MIM and thin Cr film (Fig. 3) and the emissivity of the blackbody (i.e. 1), we can plot IR spectral radiance as in Fig. 6. Since our aim is to show the change of IR radiance of the MIM and thin Cr film structures with respect to blackbody and each other at  $\lambda = 1.8 \mu\text{m}$ , temperature is set to 1610 K which corresponds to  $\lambda = 1.8 \mu\text{m}$  peak emission wavelength of the ideal blackbody according to Wien's displacement law. We notice that MIM radiance shows spectral selectivity by having near blackbody emission around  $\lambda = 1.2 \mu\text{m}$  and suppressed IR emission about 100% with respect to the blackbody and about 30% with respect to the thin Cr film around  $\lambda = 1.8 \mu\text{m}$ . On the other hand, thin Cr film looks like reduced emission with respect to blackbody but it is like graybody emission rather than spectral selection.

## Discussion

In conclusion, we have demonstrated spectrally selective IR absorption with a triple-layer MIM nanocavity structure while non-selective absorption with a thin Cr film. Occurrence of absorption peaks and dips in the MIM were explained with the electric field intensity localization with respect to the wavelength and the position of the device. It has been shown that the more electric field intensity placement in the lossy material causes enhanced power absorption while the less electric field intensity in the lossy material causes suppressed absorption. Therefore, we can manipulate IR emissive properties by controlling the electric field localization with proper design of ultra-thin lossy films either like MIM nanocavity for spectral selectivity or ultra-thin film for uniform selectivity purposes.

## Methods

**Finite-Difference-Time-Domain (FDTD) Simulations.** Absorbed power and electric field intensity in our structures and their spectral response were calculated using commercial software from Lumerical Solutions.

**Transfer Matrix Method (TMM) Calculations.** The field within each layer could be treated as superposition of forward-traveling (transmitted) and backward-traveling (reflected) wave with wave number  $k$  and a transfer matrix could represent the propagation through interface or within medium. By cascading the transfer matrix for each layer the whole system transfer matrix can be obtained, from which one could derive the transmittance  $T(\lambda)$  and reflectivity  $R(\lambda)$  of the structures.

**Fabrication of the Structures.** For the MIM structure, 100 nm Au was deposited on double side polished sapphire substrate. Then, 590 nm Poly(methyl methacrylate) (PMMA) layer was spin coated over the Au layer. Finally, 6 nm Cr was deposited on double side polished sapphire substrate (for thin Cr film) and on PMMA for the MIM.

**Optical Measurements.** Experimental reflection measurements of both structures were carried out using an infrared microscope (Bruker Hyperion 2000) and the Fourier transform infrared (FTIR) spectrometer (Bruker Vertex 70) with liquid nitrogen cooled mercury cadmium telluride and near-IR source. Reflected light was collected using Hyperion 2000 IR microscope with a  $15\times$  magnification objective and a numerical aperture of 0.4. For the calibration of the reflection measurement, we first collected the reflection from a reference gold mirror between 1 and 6  $\mu\text{m}$ . Measured reflection from the samples was then calibrated using the reflection spectra of the gold mirror. Experimental transmission of thin Cr films was measured using Fourier transform infrared (FTIR) spectrometer (Bruker Vertex 70) equipped with a room temperature triglycine sulfate (DTGS) detector. We did not measure transmission of the MIM because it has an optically thick 100 nm Au bottom metal, which prevents the light transmission.

- Kasap, S. *Optoelectronics and Photonics: Principles and Practices*. (Pearson Education, 2013).
- Landy, N., Sajuyigbe, S., Mock, J., Smith, D. & Padilla, W. Perfect metamaterial absorber. *Phys. Rev. Lett.* **100**, 207402 (2008).
- Tao, H. *et al.* A metamaterial absorber for the terahertz regime: Design, fabrication and characterization. *Opt. Express* **16**, 7181–7188 (2008).
- Avitzour, Y., Urzhumov, Y. A. & Shvets, G. Wide-angle infrared absorber based on a negative-index plasmonic metamaterial. *Phys. Rev. B* **79**, 045131 (2009).
- Liu, N., Mesch, M., Weiss, T., Hentschel, M. & Giessen, H. Infrared perfect absorber and its application as plasmonic sensor. *Nano Lett.* **10**, 2342–2348 (2010).
- Liu, X., Starr, T., Starr, A. F. & Padilla, W. J. Infrared spatial and frequency selective metamaterial with near-unity absorbance. *Phys. Rev. Lett.* **104**, 207403 (2010).
- Aydin, K., Ferry, V. E., Briggs, R. M. & Atwater, H. A. Broadband polarization-independent resonant light absorption using ultrathin plasmonic super absorbers. *Nat. Commun.* **2**, 517 (2011).
- Kats, M. A. *et al.* Ultra-thin perfect absorber employing a tunable phase change material. *Appl. Phys. Lett.* **101**, 221101 (2012).
- Kats, M. A., Blanchard, R., Genevet, P. & Capasso, F. Nanometre optical coatings based on strong interference effects in highly absorbing media. *Nat. Mater.* **12**, 20–24 (2013).
- Kats, M. A., Blanchard, R., Ramanathan, S. & Capasso, F. Thin-film interference in lossy, ultra-thin layers. *Opt. Photonics News* **25**, 40–47 (2014).
- Song, H. *et al.* Nanocavity enhancement for ultra-thin film optical absorber. *Adv. Mater.* **26**, 2737–2743 (2014).
- Ahmad, N., Stokes, J., Fox, N., Teng, M. & Cryan, M. Ultra-thin metal films for enhanced solar absorption. *Nano Energy* **1**, 777–782 (2012).
- Shu, S., Li, Z. & Li, Y. Y. Triple-layer Fabry-Perot absorber with near-perfect absorption in visible and near-infrared regime. *Opt. Express* **21**, 25307–25315 (2013).
- Cao, T., Zhang, L., Simpson, R. E. & Cryan, M. J. Mid-infrared tunable polarization-independent perfect absorber using a phase-change metamaterial. *J. Opt. Soc. Am. B* **30**, 1580–1585 (2013).
- Strecher, W., Law, S., Rooney, G., Jacobs, T. & Wasserman, D. Strong absorption and selective emission from engineered metals with dielectric coatings. *Opt. Express* **21**, 9113–9122 (2013).
- Cleary, J. W., Soref, R. & Hendrickson, J. R. Long-wave infrared tunable thin-film perfect absorber utilizing highly doped silicon-on-sapphire. *Opt. Express* **21**, 19363–19374 (2013).
- Kats, M. A. *et al.* Vanadium dioxide as a natural disordered metamaterial: perfect thermal emission and large broadband negative differential thermal emittance. *Phys. Rev. X* **3**, 041004 (2013).
- Yeh, P. *Optical Waves in Layered Media*. (Wiley, 2005).
- Palik, E. D. *Handbook of Optical Constants of Solids II*. (Elsevier Science, 1998).
- Ferry, V. E., Sweatlock, L. A., Pacifici, D. & Atwater, H. A. Plasmonic nanostructure design for efficient light coupling into solar cells. *Nano Lett.* **8**, 4391–4397 (2008).
- Talghader, J. J., Gawarikar, A. S. & Shea, R. P. Spectral selectivity in infrared thermal detection. *Light Sci. Appl.* **1**, e24 (2012).



22. Watts, C. M., Liu, X. & Padilla, W. J. Metamaterial electromagnetic wave absorbers. *Adv. Mater.* **24**, OP98–OP120 (2012).

## Acknowledgments

This research was supported by the Materials Research Science and Engineering Center (NSF-MRSEC) (DMR-1121262) of Northwestern University. K.A. acknowledges financial support from the McCormick School of Engineering and Applied Sciences at Northwestern University and partial support from the AFOSR under Award No. FA9550-12-1-0280 and the Institute for Sustainability and Energy at Northwestern (ISEN) through ISEN Equipment and Booster Awards. H.K. was supported by The Scientific and Technological Research Council of Turkey (TUBITAK) through a postdoctoral research fellowship program. This research made use of the NUANCE Center at Northwestern University, which is supported by NSF-NSEC, NSF-MRSEC, Keck Foundation, and the State of Illinois and the NUFAB cleanroom facility at Northwestern University.

## Author contributions

H.K. and K.A. conceived the idea. H.K. and Z.L. designed the structures and performed FDTD and TMM numerical electromagnetic simulations. S.B. and H.K. fabricated and

measured the structures. K.A. supervised the research. H.K. wrote the manuscript. H.K., S.B., Z.L. and K.A. edited and reviewed the manuscript.

## Additional information

**Competing financial interests:** The authors declare no competing financial interests.

**How to cite this article:** Kocer, H., Butun, S., Li, Z. & Aydin, K. Reduced near-infrared absorption using ultra-thin lossy metals in Fabry-Perot cavities. *Sci. Rep.* **5**, 8157; DOI:10.1038/srep08157 (2015).



This work is licensed under a Creative Commons Attribution-NonCommercial-NoDerivs 4.0 International License. The images or other third party material in this article are included in the article's Creative Commons license, unless indicated otherwise in the credit line; if the material is not included under the Creative Commons license, users will need to obtain permission from the license holder in order to reproduce the material. To view a copy of this license, visit <http://creativecommons.org/licenses/by-nc-nd/4.0/>